AMERICAN ACADEMY™
OF OPHTHALMOLOGY

Optical Coherence Tomography Angiography Vessel Density in Glaucomatous Eyes with Focal Lamina Cribrosa Defects

Min Hee Suh, MD,[1,2] *Linda M. Zangwill, PhD,*[1] *Patricia Isabel C. Manalastas, MD,*[1] *Akram Belghith, PhD,*[1] *Adeleh Yarmohammadi, MD,*[1] *Felipe A. Medeiros, MD, PhD,*[1] *Alberto Diniz-Filho, MD, PhD,*[1] *Luke J. Saunders, PhD,*[1] *Siamak Yousefi, PhD,*[1] *Robert N. Weinreb, MD*[1]

Purpose: To investigate whether vessel density assessed by optical coherence tomography angiography (OCT-A) is reduced in glaucomatous eyes with focal lamina cribrosa (LC) defects.

Design: Cross-sectional, case-control study.

Participants: A total of 82 patients with primary open-angle glaucoma (POAG) from the Diagnostic Innovations in Glaucoma Study (DIGS) with and without focal LC defects (41 eyes of 41 patients in each group) matched by severity of visual field (VF) damage.

Methods: Optical coherence tomography (OCT) angiography–derived circumpapillary vessel density (cpVD) was calculated as the percentage area occupied by vessels in the measured region extracted from the retinal nerve fiber layer (RNFL) in a 750-μm-wide elliptical annulus around the disc. Focal LC defects were detected using swept-source OCT images.

Main Outcome Measures: Comparison of global and sectoral (eight 45-degree sectors) cpVDs and circumpapillary RNFL (cpRNFL) thicknesses in eyes with and without LC defects.

Results: Age, global, and sectoral cpRNFL thicknesses, VF mean deviation (MD) and pattern standard deviation, presence of optic disc hemorrhage, and mean ocular perfusion pressure did not differ between patients with and without LC defects ($P > 0.05$ for all comparisons). Mean cpVDs of eyes with LC defects were significantly lower than in eyes without a defect globally (52.9%±5.6% vs. 56.8%±7.7%; $P = 0.013$) and in the inferotemporal (IT) (49.5%±10.3% vs. 56.8%±12.2%; $P = 0.004$), superotemporal (ST) (54.3%±8.8% vs. 58.8%±9.6%; $P = 0.030$), and inferonasal (IN) (52.4%±9.0% vs. 57.6%±9.1%; $P = 0.009$) sectors. Eyes with LC defects in the IT sector (n = 33) had significantly lower cpVDs than eyes without a defect in the corresponding IT and IN sectors ($P < 0.05$ for all). Eyes with LC defects in the ST sector (n = 19) had lower cpVDs in the ST, IT, and IN sectors ($P < 0.05$ for all).

Conclusions: In eyes with similar severity of glaucoma, OCT-A-measured vessel density was significantly lower in POAG eyes with focal LC defects than in eyes without an LC defect. Moreover, reduction of vessel density was spatially correlated with the location of the LC defect. *Ophthalmology 2016;■:1–9 © 2016 by the American Academy of Ophthalmology.*

Although the pathogenesis of glaucoma is not fully understood, the lamina cribrosa (LC) is a putative site of retinal ganglion cell axonal injury.[1–4] Focal LC defects, areas of localized loss of laminar tissue, recently have been reported to be an important structural feature associated with glaucomatous visual field (VF) loss.[5–7] Furthermore, there is increasing evidence that focal LC defects may be related to vascular changes of the optic nerve head (ONH), including optic disc hemorrhage,[7–9] as well as other ophthalmoscopic structural changes such as neuroretinal rim loss, acquired pits of the ONH, and retinal nerve fiber layer (RNFL) defects.[10,11] However, little is known about the association between the retinal microvasculature and the presence of focal LC defects, an issue relevant to the pathogenesis of glaucomatous optic neuropathy.[12,13]

Optical coherence tomography angiography (OCT-A) is now available to provide qualitative and quantitative information of the perfused microvasculature of various retinal layers. It has advantages over other techniques, such as fluorescein angiography, laser speckle flowgraphy, and laser Doppler flowmetry by its noninvasiveness and better reproducibility.[14–20] Furthermore, OCT-A-derived quantification of the peripapillary vasculature has been shown to be related to the presence and severity of the glaucoma.[14–16,21]

http://dx.doi.org/10.1016/j.ophtha.2016.07.023
ISSN 0161-6420/16

The purpose of this study was to compare the OCT-A-derived peripapillary RNFL vessel density between glaucomatous eyes with and without a focal LC defect.

Methods

Study Subjects

This was a cross-sectional study involving patients with primary open-angle glaucoma (POAG) from the Diagnostic Innovations in Glaucoma Study (DIGS) (ClinicalTrials.gov identifier: NCT00221897). The DIGS is an ongoing prospective, longitudinal study at the Hamilton Glaucoma Center, University of California, San Diego, designed to evaluate optic nerve structure and visual function in glaucoma. Details of the DIGS protocol have been described.[22] All methods adhered to the tenets of the Declaration of Helsinki and the Health Insurance Portability and Accountability Act and were approved by the institutional review boards at the University of California, San Diego. Informed consent was obtained from all participants.

Patients with established POAG who completed OCT-A imaging and ONH imaging using both spectral-domain OCT (SD OCT) and swept-source OCT (SS-OCT) were included. All participants underwent an ophthalmological examination, including assessment of best-corrected visual acuity (BCVA), slit-lamp biomicroscopy, intraocular pressure (IOP) measurement with Goldmann applanation tonometry, gonioscopy, central corneal thickness measured with ultrasound pachymetry (DGH Technology Inc., Exton, PA), dilated fundus examination, simultaneous stereophotography of the optic disc, standard automated perimetry (Humphrey Field Analyzer; 24-2 Swedish interactive threshold algorithm; Carl Zeiss Meditec, Dublin, CA), SD OCT, OCT-A, and SS-OCT. Perimetry and all imaging tests were conducted within a 6-month period.

To be included, patients were required to have been diagnosed with POAG, to be aged >18 years, to have BVCA ≥20/40, and to have an open angle on gonioscopy. Patients with a history of ocular intervention (except for uncomplicated cataract or glaucoma surgery), intraocular disease (e.g., diabetic retinopathy or non-glaucomatous optic neuropathy), or systemic disease (e.g., stroke or pituitary tumor) that could influence the study results were excluded from the study. Those with systemic hypertension and diabetes mellitus were included unless they were diagnosed with diabetic or hypertensive retinopathy. Eyes with unreliable VF or poor quality imaging tests also were excluded.

Primary open-angle glaucoma was defined as the presence of glaucomatous optic nerve damage (i.e., the presence of focal thinning, notching, or localized or diffuse atrophy of the RNFL) and associated repeatable VF damage. Glaucomatous VF damage was defined as a glaucoma hemifield test outside normal limits or a pattern standard deviation outside 95% normal limits confirmed on 2 consecutive, reliable (fixation losses and false-negatives ≤33% and ≤15% false-positives) tests.

Systemic measurements included systolic and diastolic blood pressure and pulse rate measured at the height of the heart with an Omron Automatic blood pressure instrument (model BP791IT; Omron Healthcare, Inc., Lake Forest, IL). Mean arterial pressure was calculated as 1/3 systolic blood pressure + 2/3 diastolic blood pressure. Mean ocular perfusion pressure was defined as the difference between 2/3 of mean arterial pressure and IOP.

Presence of the disc hemorrhage was determined on the basis of stereophotography that had been obtained previously at intervals of 12 months. Glaucomatous disc hemorrhage was defined as an isolated splinter or flame-shaped hemorrhage on optic disc tissue or crossing the optic disc.[23] Two independent graders who were masked to patient information and test results independently evaluated each image. Discrepancies between the 2 graders were resolved by consensus.

Spectral-Domain Optical Coherence Tomography Imaging

All subjects underwent ONH imaging with a commercial SD OCT system (Avanti; Optovue, Inc., Fremont, CA). Avanti SD OCT has an A-scan rate of 70 kHz and a light source with a center wavelength of 840 nm. The ONH map protocol calculates circumpapillary RNFL (cpRNFL) thicknesses in a 10-pixel-wide band along a 3.45-mm-diameter circle centered on the ONH based on the 360-degree global area and eight 45-degree sectors. Only good-quality images, defined as scans with a signal strength index ≥37 and without segmentation failure or artifacts, were included.

Optical Coherence Tomography Angiography Imaging

The OCT AngioVue system (Optovue, Inc.) incorporated in the Avanti SD OCT system provides noninvasive visualization of the retinal microvasculature. Details have been described by Jia et al.[14] Briefly, the OCT-A image is directly derived from SD OCT B-scans. Specifically, the SD OCT image consists of a series of B-scans with 2 rapid repeats at each B-scan location, and the average of the 2 repeated B-scans forms the conventional SD OCT intensity image. The amplitude decorrelation between these 2 B-scans forms the OCT-A image. Because the OCT-A image and SD OCT intensity image are based on the same B-scans, there is pixel-to-pixel co-localization between the OCT-A image volume and the SD OCT intensity image, and no need for alignment. In addition, the AngioVue system uses a split-spectrum amplitude-decorrelation angiography (SSADA) method to capture the dynamic motion of the red blood cells and provide a high-resolution 3-dimensional visualization of perfused retinal microvasculature[14,21,24,25] (Figs 1 and 2A-3 and B-3). The microvascular information is characterized at various user-defined retinal layers as a vessel density map. Then, vessel density (percentage) is calculated as the proportion of the measured area occupied by flowing blood vessels (defined as pixels having decorrelation values acquired by the SSADA algorithm above the threshold level)[21] (Figs 1 and 2A-3 and B-3).

In this study, circumpapillary vessel density (cpVD) was calculated in the RNFL and measured in a region defined as a 750-μm-wide elliptical annulus extending from the optic disc boundary based on the 360-degree global area and eight 45-degree sectors[21] (Figs 1 and 2A-3 and B-3).

Image quality of all scans was reviewed according to a standard protocol established by the Imaging Data Evaluation and Analysis reading center at the Hamilton Glaucoma Center. Trained graders reviewed scans, and those with poor image quality, as defined by the following criteria, were excluded: (1) a signal strength index <48 (1 = minimum, 100 = maximum), (2) poor clarity, (3) residual motion artifacts visible as an irregular vessel pattern or disc boundary on the en face angiogram, (4) a local weak signal, and (5) RNFL segmentation errors. The delineation of the disc margin was reviewed for accuracy and adjusted manually, if required.[21]

Swept-Source Optical Coherence Tomography Imaging

For detecting focal LC defects, the optic disc was imaged with SS-OCT (DRI-OCT; Topcon, Tokyo, Japan). This device has an image-acquisition rate of 100 000 A-scans/second using a light

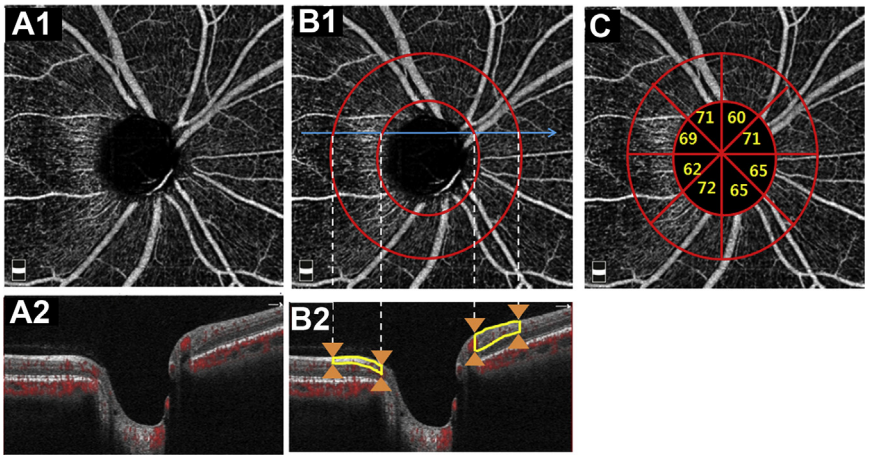

Figure 1. Analysis of circumpapillary retinal nerve fiber layer vessel density (cpVD) based on optic nerve head (ONH) optical coherence tomography angiography (OCT-A) images. **A**, En face (**A-1**) and horizontal (**A-2**) images of the radial peripapillary capillaries within the retinal nerve fiber layer (RNFL). **B-1**, Same en face image as **A-1** but annotated to indicate a 750-μm-wide elliptical annulus (*red circles*) extending from the optic disc boundary that forms the region of analysis for cpVD and the location of the B-scan shown in **B-2** (*sky blue lines*). **B-2**, B-scan view of the vessel density analysis region located within the elliptical annulus (*orange arrows*) and within the depth range of the RNFL layer (*yellow outlines*). **C**, Same en face image as **A-1** and **B-1**, but annotated to indicate eight 45-degree sectors for cpVD.

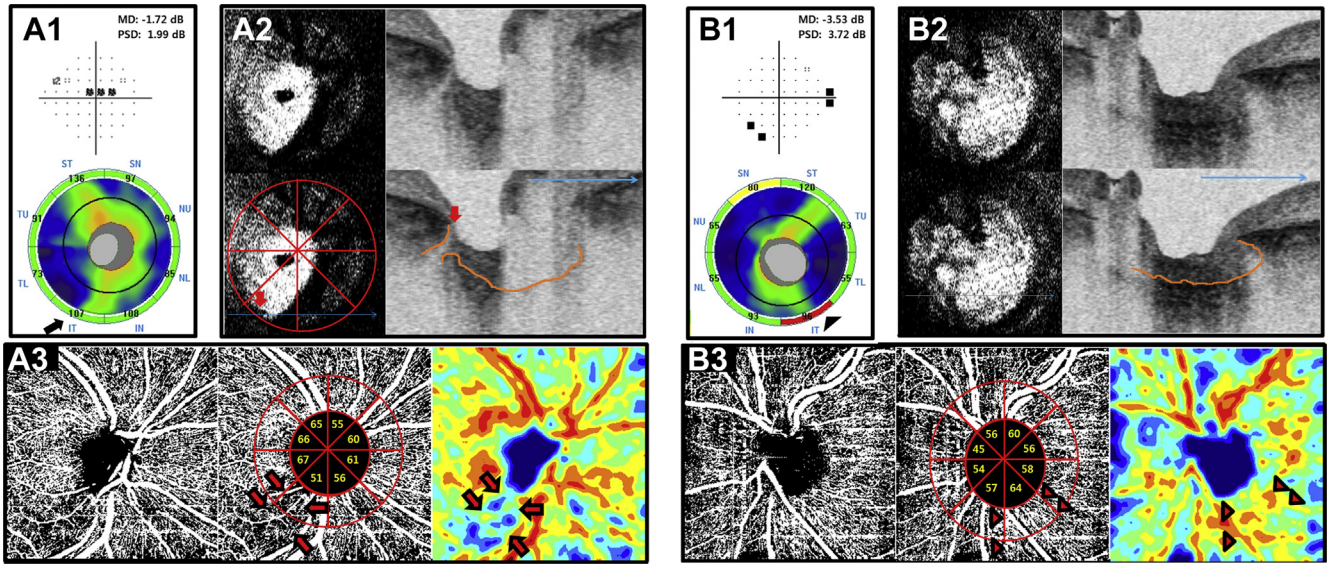

Figure 2. An optical coherence tomography angiography (OCT-A)—derived vessel density map in subjects with primary open-angle glaucoma (POAG) with (**A**) and without (**B**) a focal lamina cribrosa (LC) defect. **A-1** and **B-1**, Visual field (VF) (**top**) and circumpapillary retinal nerve fiber layer (RNFL) thickness on the spectral-domain optical coherence tomography (SD OCT) image (**bottom**) of the right eye with a focal LC defect (**A-1**) and the left eye without an LC defect (**B-1**). Note that the eye with an LC defect did not show RNFL thinning (all RNFL sectors were within normal limits) on the circular diagram (*black arrow*) (**A-1 bottom**), whereas the eye without an LC defect showed an RNFL defect (outside normal limit) in the inferotemporal (IT) sector (*black arrowhead*) (**B-1 bottom**). **A-2** and **B-2**, En face (**left**) and horizontal (**right**) B-scan images of the swept source (SS)-OCT from eyes with (**A-2**) and without (**B-2**) an LC defect. **Bottom** images are the same as **top** images without labels and contain an 8-sector face circle, with *orange lines* delineating the anterior LC surface and large *sky blue arrows* indicating the horizontal scan direction. A focal LC defect was located in the IT sector (*red arrows*) on SS-OCT (**A-2**). **A-3** and **B-3**, The circumpapillary RNFL vessel density map of eyes with (**A-3**) and without (**B-3**) an LC defect. **Center** images are the same as those on the **left** but are annotated to include the 8-sector circle with vessel density values for each sector. **Right** images show color-coded maps. The eye with an LC defect showed notable vessel density reduction (*black-outlined red arrows*) in the corresponding IT sector (**A-3**), whereas the eye without a defect showed no evidence of focal vessel density reduction in the IT sector (*black-outlined red arrowheads*) (**B-3**). MD = mean deviation; PSD = pattern standard deviation.

source with a center wavelength of 1050 nm. Details on the device have been described by other investigators.[26–28]

A 3-dimensional raster scan consisting of 256 serial horizontal B-scans over 12×9-mm cube centered on the posterior pole (wide-field protocol) was acquired,[28] and serial en face images were obtained from the 3-dimensional data set.

Poor-quality images (quality score <50, clipped or poorly focused scans) due to media opacity, irregular tear film, or inadequate patient cooperation were excluded.[28] Eyes with poor visibility of the LC, defined as <70% visibility of the anterior laminar surface within the Bruch's membrane opening, also were excluded from analysis.[9] Two independent observers (M.H.S. and P.I.C.M.) masked to the clinical information of the study subjects carefully reviewed the obtained horizontal and en face SS-OCT images for the presence of focal LC defects. Discrepancies between the 2 observers were resolved by consensus. If consensus could not be reached, the subject was excluded from the analysis. A focal LC defect was defined as a laminar hole or laminar disinsertions violating the normal U- or W-shaped contour of the anterior laminar surface.[6–11,29] To avoid false-positives, focal LC defects were required to be ≥100 μm in diameter and >30 μm in depth, and to be present on at least 2 consecutive scans.[6,7,10,11,29] Observers also confirmed that the candidate LC defects did not correspond with the hyporeflectivity due to vascular shadowing by comparing the en face images with the disc photographs.

Location of the LC defect was described in terms of eight 45-degree sectors corresponding to the sectors on the SD OCT Avanti and AngioVue instruments (Fig 2A-2, -3 and B-2, -3). An 8-sector face circle was placed around the ONH on the SS-OCT en face image after matching its location with that of the AngioVue cpVD circular diagram registering the images by matching the location of the vessels. Then, a sector in which the defect was located was assigned. If the subject had an LC defect located over 2 neighboring sectors, only 1 sector that involved the larger portion of a defect was assigned.

If both eyes of each patient with POAG had focal LC defects or were free of focal LC defects, 1 eye from the patient was randomly selected for analysis. If a patient had 1 eye with and 1 eye without a focal LC defect, the eye with the focal LC defect was included. Subjects with POAG without a focal LC defect were matched to those with defects for VF mean deviation (MD) to minimize the influence of the glaucoma severity on LC defect, cpRNFL thickness, and vessel density. Specifically, patients with focal LC defects were matched to patients without LC defect in 3 groups based on the severity of their VF damage: 27 with early POAG (MD >−6 decibels [dB]), 8 with moderate POAG (−12 dB ≤ MD ≤−6 dB), and 6 with advanced POAG (MD <−12 dB) using the frequency matching method.[30]

Data Analysis

Clinical characteristics, OCT-derived cpRNFL thicknesses, and OCT-A-derived vessel densities were compared between glaucomatous eyes with and without focal LC defects. Normality assumption was assessed by inspecting histograms and using Shapiro–Wilk tests. An independent samples Student *t* test was used for group comparison for normally distributed variables, the Mann–Whitney test was used for continuous non-normal variables, and the chi-square test was used for categoric variables. To evaluate interobserver agreement for the presence of focal LC defects, the kappa coefficient was calculated.[11,31,32] All statistical analyses were performed with JMP version 11.2.0 (SAS Institute Inc., Cary, NC) and MedCalc (MedCalc, Inc., Mariakerke, Belgium). The α level (type I error) was set at 0.05.

Results

Among 180 eyes of 138 patients with POAG who were initially enrolled, 36 eyes of 21 patients were excluded because of poor-quality OCT-A (34 eyes of 19 patients) or SD OCT ONH (2 eyes of 2 patients) images. Among the remaining 144 eyes of the 117 patients, 6 eyes (4.2%) of 3 patients were excluded because of not having SSOCT images, 13 eyes (9.0%) of 11 patients were excluded because of poor-quality SS-OCT images, and 1 eye (0.69%) of 1 patient was excluded because the 2 observers failed to reach a consensus in determining the presence of an LC defect. There remained 55 eyes of 42 patients with LC defects and 69 eyes of 60 patients without an LC defect. After frequency matching VF MD between patients with and without LC defects, 41 eyes of 41 patients with POAG were included in each group. There was an excellent interobserver agreement in determining the presence of the LC defect in these 82 eyes (kappa = 0.84; 95% confidence interval, 0.76–0.91; $P < 0.001$).[32,33]

Demographics and characteristics of ophthalmic measurements are summarized in Table 1. There were no significant differences between patients with and without LC defects in the baseline clinical and ocular characteristics, including age, diabetes mellitus, systemic hypertension, systemic antihypertensive and diabetes medications, number and type of topical glaucoma medications, IOP, mean ocular perfusion pressure, presence of disc hemorrhage, VF MD, and global and sectoral RNFL thicknesses ($P > 0.05$) (Table 1).

Among 41 eyes with focal LC defects, 33 eyes (80%) had defects located in the inferotemporal (IT) sector, 19 eyes (46%) had defects located in the superotemporal (ST) sector, 1 eye (2%) had defects located in the inferonasal (IN) sector, and 1 eye (2%) had defects located in the superonasal sector. The LC defects were detected in both ST and IT sectors in 12 eyes (29%) and in both IN and IT sectors in 1 eye (2%).

Table 2 presents the OCT-A-derived vessel densities according to the presence of LC defects. Eyes with focal LC defects had significantly lower cpVDs than eyes without a defect in the global area (52.9%±5.6% vs. 56.8%±7.7%; $P = 0.013$) and in the IT (49.5%±10.3% vs. 56.8%±12.2%; $P = 0.004$), ST (54.3%±8.8% vs. 58.8%±9.6%; $P = 0.030$), and IN (52.4%±9.0% vs. 57.6%±9.1%; $P = 0.009$) sectors. The 2 groups did not differ significantly with respect to the cpVDs of all other sectors ($P > 0.05$) (Table 2).

Subgroup analysis of 33 eyes with LC defects in the IT sector showed significantly lower cpVDs than eyes without a defect in the IT and IN sectors, with sectoral differences highest in the IT (49.1%±10.3% vs. 56.8%±12.2%; $P = 0.005$) followed by the IN (53.0%±9.00% vs. 57.6%±9.1%; $P = 0.035$) sectors (Figs 2 and 3A). The subset of 19 eyes with LC defects in the ST sector had lower cpVDs in the ST, IT, and IN sectors, and sector differences were highest in the ST sector (50.8%±9.4% vs. 58.8%±9.6%; $P = 0.004$), followed by the IT (49.1%±11.9% vs. 56.8%±12.2%; $P = 0.026$) and IN (51.4%±10.4% vs. 57.9%±9.1%; $P = 0.023$) sectors (Fig 3B). Mean global and sectoral cpRNFL thicknesses of the 2 subgroups with LC defects in the ST and IT sectors did not differ from those without a defect ($P > 0.05$).

Discussion

In this study, OCT-A-based cpVDs measured in the RNFL were significantly lower in glaucomatous eyes with focal LC defects compared with eyes without LC defects, whereas glaucoma severity did not differ between the 2 groups.

Table 1. Subject Demographics and Baseline Clinical Characteristics

Variables	Eyes with Focal LC Defect (41 Eyes, 41 Patients)	Eyes without Focal LC Defect (41 Eyes, 41 Patients)	*P* Value
Age (yrs)	73.4±14.0 (36–94)	72.0±9.5 (51–89)	0.235*
Gender (male/female)	20/21	24/17	0.507†
SE (D)	−0.95±2.2 (−8.4 to 2.3)	−0.94±1.7 (−5.1 to 2.9)	0.568*
CCT (μm)	529.1±42.3 (460.3–606.0)	532.3±40.7 (425.3–619.0)	0.739‡
Ethnicity (ASD/ED/AFD), n	9/24/8	3/29/9	0.171†
Self-reported diabetes, n (%)	6 (14.6)	4 (9.8)	0.736†
Self-reported hypertension, n (%)	22 (53.7)	19 (46.3)	0.659†
Antihypertensive medication, n (%)	17 (41.5)	16 (39.0)	1.000†
Diabetes medication, n (%)	5 (12.2)	3 (7.3)	0.710†
Topical glaucoma medications, n (%)			
0	1 (2.4)	4 (9.8)	0.246†
1	16 (39.0)	11 (26.8)	
>1	24 (58.5)	26 (63.4)	
Topical medications, n			
Prostaglandin analogues	31	30	0.990†
Beta-antagonists	16	17	
Carbonic anhydrase inhibitors	6	7	
Alpha-1 antagonists	20	20	
IOP (mmHg)	13.5±5.7 (4–30)	13.1±4.4 (4–26)	0.787‡
SBP (mmHg)	127.1±14.2 (92–162)	121.9±12.8 (98–151)	0.083‡
DBP (mmHg)	77.5±11.3 (51–108)	75.9±9.2 (51–100)	0.474‡
MOPP (mmHg)	54.7±8.6 (35.1–75.8)	52.5±6.2 (39.3–66.7)	0.197‡
Pulse rate (beats/min)	67.9±12.4 (46–108)	66.0±11.4 (41–85)	0.767*
Disc hemorrhage, n (%)	4 (9.8)	7 (17.1)	0.517†
VF MD (dB)	−6.60±6.02 (−25.87 to −0.41)	−5.82±6.08 (−26.24 to −0.30)	0.252*
VF PSD (dB)	6.60±3.96 (1.71–14.57)	5.63±3.69 (1.82–14.37)	0.286*
Disc area (mm^2)	2.2±0.4 (1.4–3.2)	2.0±0.53 (0.93–3.0)	0.156‡
RNFL thickness, μm			
Global area	72.2±10.2 (51.9–98.9)	73.7±14.1 (41.5–110.7)	0.576‡
Upper temporal	60.4±14.7 (31.6–93.8)	60.0±15.4 (31.7–86.7)	0.895‡
Upper nasal	64.6±12.8 (43.2–98.7)	62.9±13.1 (32.0–105.5)	0.558‡
Lower nasal	61.3±11.2 (36.9–88.1)	59.8±11.1 (35.8–81.6)	0.554‡
Lower temporal	53.6±9.7 (35.7–84.8)	55.0±14.4 (28.1–103.6)	0.608‡
ST	95.2±21.0 (56.0–136.3)	97.0±23.3 (50.2–144.1)	0.714‡
SN	81.9±14.7 (48.2–113.9)	81.9±20.8 (52.3–138.0)	0.901‡
IN	80.3±20.4 (48.8–139.3)	84.7±23.1 (40.7–135.7)	0.366‡
IT	80.6±21.4 (50.9–127.9)	88.1±25.7 (46.6–142.6)	0.154*

AFD = African descent; ASD = Asian descent; CCT = central corneal thickness; D = diopters; dB = decibels; DBP = diastolic blood pressure; ED = European descent; IN = inferonasal; IOP = intraocular pressure; IT = inferotemporal; LC = lamina cribrosa; MOPP = mean ocular perfusion pressure; RNFL = retinal nerve fiber layer; SBP = systolic blood pressure; SE = spherical equivalent; SN = superonasal; ST = superotemporal; VF MD = visual field mean deviation; VF PSD = visual field pattern standard deviation.
Continuous variables are shown as mean ± standard deviation (range).
*Comparison was performed by using the Mann–Whitney test.
†Comparison was performed by using the chi-square test.
‡Comparison was performed by using independent samples *t* test.

Lower cpVD was most pronounced in the ST and IT sectors and, most important, showed a topographic relationship with the location of the LC defect. This investigation provides potentially important perspectives regarding the relationship between the retinal microvasculature and the focal LC defects.

The LC is a porous structure through which retinal ganglion cell axons and retinal blood vessels pass,[2–4] and focal LC damage has been associated with axonal and vascular damage.[6–11] There is increasing evidence that various clinical signs of axonal loss, such as an RNFL defect, neuroretinal rim thinning/notching, and acquired pits of the ONH, may be related to focal LC damage.[5,7,10,11,29] Until recently, the relationship between LC defects and retinal microvasculature has been difficult to evaluate because in vivo imaging of the microvasculature at specific retinal layers was not possible. For example, it only could be inferred that a focal LC defect is related to the presence of a disc hemorrhage detected on disc photographs.[7–9] With OCT-A, we now are able to demonstrate that peripapillary vessel density in eyes with a similar severity of POAG was significantly lower when there is a focal LC defect than when there is not an LC focal defect. The current findings are consistent with previous studies suggesting that focal LC defects and impaired ocular hemodynamics may be etiologically related, and that mechanical and vascular mechanisms of glaucomatous optic nerve injury are inseparably intertwined.[12,13]

Table 2. Comparison of Optical Coherence Tomography Angiography–Derived Circumpapillary Vessel Density Values between the Primary Open-Angle Glaucoma Subjects with and without a Focal Lamina Cribrosa Defect in Global Area and in Eight 45-Degree Sectors

	Eyes with Focal LC Defect (41 Eyes, 41 Patients)		Eyes without Focal LC Defect (41 Eyes, 41 Patients)	
	*N**	*OCT-A Parameters (%)*	*OCT-A Parameters (%)*	***P* Value**
Global area	–	52.9±5.6 (42.4–63.1)	56.8±7.7 (35.4–71.5)	**0.013**†
Upper temporal	0	57.1±9.9 (32.9–72.6)	60.0±9.9 (38.0–73.4)	0.107‡
Upper nasal	0	50.9±6.9 (33.6–62.5)	54.1±9.2 (31.9–71.4)	0.077†
Lower nasal	0	52.7±6.9 (36.4–63.3)	52.7±6.9 (32.3–66.9)	0.383†
Lower temporal	0	54.2±9.3 (34.8–70.9)	57.1±9.4 (29.7–74.8)	0.155†
ST	19	54.3±8.8 (33.7–69.7)	58.8±9.6 (33.8–73.1)	**0.030**†
SN	1	53.5±6.7 (40.3–65.8)	55.9±7.9 (30.2–70.4)	0.133†
IN	1	52.4±9.0 (33.2–66.7)	57.6±9.1 (32.3–74.1)	**0.009**†
IT	33	49.5±10.3 (28.0–66.8)	56.8±12.2 (31.8–76.0)	**0.004**†

IN = inferonasal; IT = inferotemporal; LC = lamina cribrosa; OCT-A = optical coherence tomography angiography; SN = superonasal; ST = superotemporal.
Continuous variables are shown as mean ± standard deviation (range).
Significant values are in bold type.
*N = number of eyes with focal LC defects in each of eight 45-degree sectors.
†The OCT-A parameters between eyes with and without a focal LC defect were compared using independent samples *t* test.
‡The OCT-A parameters between eyes with and without a focal LC defect were compared using the Mann–Whitney test.

This study also confirms previous results that focal LC defects are located mostly in the IT area followed by the ST area of the ONH.[9,11,29] Likewise, significantly lower OCT-A-derived cpVD was notable in these areas. Furthermore, subgroup analysis in eyes with LC defects at the ST and IT sectors showed that the location of the lowest vessel density corresponded topographically to the location of the LC defect. A subset of eyes with LC defects at the ST sector had lower vessel density in the contralateral IT and IN sectors, as well as in the corresponding ST sector. This may be because 63.2% (12/19) of those with LC defects in the ST area also had defects in the IT area. These findings suggest that detectable structural and microvascular damage to the optic disc is spatially correlated.[8]

One possible explanation for the temporal relationship between the laminar and microvascular changes is that loss of structural support of the laminar beams due to the focal LC defect may directly or indirectly influence local retinal microvasculature.[3,7,33–36] Conversely, impaired vascular supply to the laminar beams may lead to the focal disruption of the laminar structures. These speculations cannot be confirmed in this study because of its cross-sectional design. Longitudinal studies are needed to elucidate the temporal relationship between the development of focal LC defects and reduced peripapillary vessel density.

The current OCT-A provides good-quality images of the microvasculature located within the peripapillary RNFL, but not for those within the ONH deep structures due to projection artifacts in which the superficial blood vessels project to deeper tissue. Vessel density specific to the neuroretinal rim tissue also is not provided with existing software. Moreover, our analysis is focused on the microvasculature within the cpRNFL, which is measured outside of the optic disc margin and therefore does not contain rim tissue. The measurement within the cpRNFL captures the radial peripapillary capillaries, vessels suggested to play a role in the pathophysiology of POAG.[21,37–40] Further studies with improved OCT-A assessment and objective criteria in determining the microvascular dropout in ONH structures are needed to further assess this hypothesis.

One may argue that adjustment for multiple testing should be applied for comparing each global area and sector-wise vessel density parameter between eyes with and without focal LC defect. In this study, eyes with focal LC defects had significantly lower cpVD than eyes without defects in the IT sector ($P = 0.004$) (Table 2), even after applying Bonferroni correction with a cutoff P value of 0.005, which is known to be a conservative method of controlling multiple comparisons.[41] When a less stringent correction method introduced by Benjamini and Hochberg[42] was applied, global area (adjusted $P = 0.043$) and the IN (adjusted $P = 0.043$) and IT (adjusted $P = 0.040$) sectors remained statistically significant. Therefore, it is less likely that differences of the cpVD values between eyes with and without focal LC defects were observed by chance.

Study Limitations

Optic disc hemorrhage, a vascular parameter associated with the presence and progression of glaucoma,[23] is known to be related to the presence of a focal LC defect.[7,8] However, in this study, the prevalence of the disc hemorrhage did not differ between eyes with and without defects. These results may be due to the relatively small number of disc hemorrhages (n = 11) detected in our study population. It is also possible that matching of the glaucomatous eyes with and without LC defects by glaucoma severity (VF MD) made the groups more similar with respect to the RNFL thickness or presence of disc hemorrhages.[7,14,16] However, although not statistically significant, eyes with LC defects tended to have worse VF MDs (−6.60±6.02 and −5.82±6.08 dB, respectively; $P = 0.252$) and thinner RNFL (72.2±10.2 and 73.7±14.1 μm,

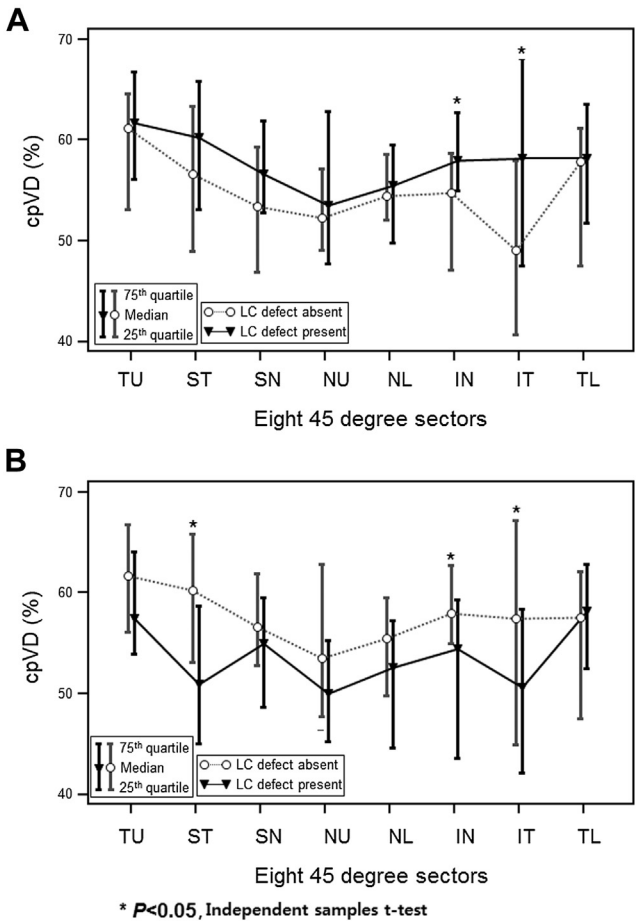

Figure 3. Comparison of optical coherence tomography angiography (OCT-A) circumpapillary vessel density (cpVD) profiles between glaucomatous eyes with and without a focal lamina cribrosa (LC) defect. **A**, Subset of 33 eyes with an LC defect located in the inferotemporal sector (IT) sector had significantly lower cpVDs in the IT and inferonasal (IN) sectors compared with those without a defect. Sector differences were highest in the IT sector. **B**, Subset of 19 eyes with an LC defect in the superotemporal (ST) sector had significantly lower cpVDs in the ST, IN, and IT sectors compared with those without a defect. Sector differences were highest in the ST sector. NL = lower nasal sector; NU = upper nasal; SN = superonasal; TL = lower temporal; TU = upper temporal.

respectively, for global cpRNFL thickness; $P = 0.576$) than eyes without a defect, suggesting that the influence of axonal loss on vessel density cannot be completely ruled out. Moreover, matching the glaucoma severity between eyes with and without focal LC defects resulted in an overlap in the distribution of the VF MDs, RNFL thickness, and vessel density values between the 2 groups. The VF MDs and RNFL thicknesses were not significantly different between the 2 groups (by design). However, despite a large overlap in the cpVD values in eyes with and without LC defects, there was a significant difference between the 2 groups. The clinical utility of the difference is not clear. Longitudinal studies are needed to determine the temporal relationship between microvascular dropout and LC defects. Patient matching also led to a relatively small sample size and thus may limit the generalizability of the current results to the general population with glaucoma. Another limitation is that focal LC defects were based on subjective observation, and even with SSOCT it is sometimes challenging to visualize the deep ONH structures. However, this limitation was addressed at least in part by having 2 graders determine the presence of LC defects, by the excellent interobserver agreement in determining the presence of the LC defect (kappa = 0.84), and by the lower exclusion rate of the poor-quality SS-OCT images (9.0%) compared with previous studies ranging between 20.0% and 25.7%.[8,10,11] The use of the en face SS-OCT images, which provided clearer visualization of the LC, may have contributed to the high interobserver agreement and low exclusion rate of the current study.[9] Third, this study had a relatively high number of poor-quality OCT-A images (34/180 [18.9%]). The current OCT-A is a newly introduced technique and does not have an eye-tracking system. Approximately 13.3% (24/180) of scans in this study were excluded because of excessive movement. Further application of the eye tracking system may help obtain better-quality OCT-A images. Fourth, the current OCT-A technique generates a binary image of the vessels based on the amplitude decorrelation between rapidly repeated B-scans. Therefore, vessels without flow may not be visualized because of lack of motion contrast. Finally, the use of 2 different devices and 8 relatively large sectors may not facilitate accurate registration between the location of the focal LC defect and the vessel density reduction. The current OCT-A software only provides cpRNFL vessel density globally and in 8 fixed 45-degree sectors. Moreover, the current SD OCT (Avanti) in which OCT-A (AngioVue) software is incorporated does not have an enhanced depth imaging technique that allows detailed analysis of the laminar structure; therefore, we used SS-OCT for the lamina analysis. However, the OCT-A image is directly derived from SD OCT B-scans. Moreover, because SSOCT and SD OCT images were aligned by matching the large vessels, it is unlikely that there is a significant error in evaluating the topographic relationship between vessel density and focal LC defects. Further development of OCT-A software that allows for location-specific vessel density measures and enhanced depth imaging is needed to more precisely map the location of microvasculature dropout to lamina defects.

In conclusion, cpVD was significantly lower in glaucomatous eyes with focal LC defects than in eyes without focal LC defects, especially in the ST and IT sectors. Moreover, lower vessel density was spatially correlated with the location of the LC defect. Longitudinal studies are needed to determine the temporal relationship between the structural alteration of the LC and the retinal microvasculature.

References

1. Weinreb RN, Aung T, Medeiros FA. The pathophysiology and treatment of glaucoma: a review. JAMA 2014;311:1901–11.
2. Fechtner RD, Weinreb RN. Mechanisms of optic nerve damage in primary open angle glaucoma. Surv Ophthalmol 1994;39:23–42.

3. Anderson DR. Ultrastructure of human and monkey lamina cribrosa and optic nerve head. Arch Ophthalmol 1969;82:800–14.
4. Wilczek M. The lamina cribrosa and its nature. Br J Ophthalmol 1947;31:551–65.
5. Quigley HA, Addicks EM. Regional differences in the structure of the lamina cribrosa and their relation to glaucomatous optic nerve damage. Arch Ophthalmol 1981;99:137–43.
6. Faridi OS, Park SC, Kabadi R, et al. Effect of focal lamina cribrosa defect on glaucomatous visual field progression. Ophthalmology 2014;121:1524–30.
7. Park SC, Hsu AT, Su D, et al. Factors associated with focal lamina cribrosa defects in glaucoma. Invest Ophthalmol Vis Sci 2013;54:8401.
8. Lee EJ, Kim TW, Kim M, et al. Recent structural alteration of the peripheral lamina cribrosa near the location of disc hemorrhage in glaucoma. Invest Ophthalmol Vis Sci 2014;55:2805–15.
9. Kim YK, Park KH. Lamina cribrosa defects in eyes with glaucomatous disc haemorrhage. Acta Ophthalmologica 2015 Nov 2. http://dx.doi.org/10.1111/aos.12903 [Epub ahead of print].
10. You JY, Park SC, Su D, et al. Focal lamina cribrosa defects associated with glaucomatous rim thinning and acquired pits. JAMA Ophthalmol 2013;131:314.
11. Tatham AJ, Miki A, Weinreb RN, et al. Defects of the lamina cribrosa in eyes with localized retinal nerve fiber layer loss. Ophthalmology 2014;121:110–8.
12. Burgoyne CF, Crawford Downs J, Bellezza AJ, et al. The optic nerve head as a biomechanical structure: a new paradigm for understanding the role of IOP-related stress and strain in the pathophysiology of glaucomatous optic nerve head damage. Prog Retin Eye Res 2005;24:39–73.
13. Downs C, Roberts MD, Burgoyne CF. Mechanical strain and restructuring of the optic nerve head. In: Shaarawy TM, Sherwood MB, Hitchings RA, Crowston JG, eds. Glaucoma Medical Diagnosis and Therapy. Vol. 1. Philadelphia, PA: Saunders Elsevier; 2009.
14. Jia Y, Wei E, Wang X, et al. Optical coherence tomography angiography of optic disc perfusion in glaucoma. Ophthalmology 2014;121:1322–32.
15. Liu L, Jia Y, Takusagawa HL, et al. Optical coherence tomography angiography of the peripapillary retina in glaucoma. JAMA Ophthalmol 2015;133:1045.
16. Wang X, Jiang C, Ko T, et al. Correlation between optic disc perfusion and glaucomatous severity in patients with open-angle glaucoma: an optical coherence tomography angiography study. Graefes Arch Clin Exp Ophthalmol 2015;253:1557–64.
17. Aizawa N, Yokoyama Y, Chiba N, et al. Reproducibility of retinal circulation measurements obtained using laser speckle flowgraphy-NAVI in patients with glaucoma. Clin Ophthalmol 2011;5:1171–6.
18. Nicolela MT, Hnik P, Schulzer M, Drance SM. Reproducibility of retinal and optic nerve head blood flow measurements with scanning laser Doppler flowmetry. J Glaucoma 1997;6:157–64.
19. Iester M, Altieri M, Michelson G, et al. Intraobserver reproducibility of a two-dimensional mapping of the optic nerve head perfusion. J Glaucoma 2002;11:488–92.
20. Hitchings RA, Spaeth GL. Fluorescein angiography in chronic simple and low-tension glaucoma. Br J Ophthalmol 1977;61:126–32.
21. Yarmohammadi A, Zangwill LM, Diniz-Filho A, et al. Optical coherence tomography angiography vessel density in healthy, glaucoma suspects, and glaucoma. Invest Ophthalmol Vis Sci 2016;57:OCT451–9.
22. Sample PA, Girkin CA, Zangwill LM, et al. The African Descent and Glaucoma Evaluation Study (ADAGES): design and baseline data. Arch Ophthalmol 2009;127:1136–45.
23. Suh MH, Park KH. Pathogenesis and clinical implications of optic disk hemorrhage in glaucoma. Surv Ophthalmol 2014;59:19–29.
24. Jia Y, Tan O, Tokayer J, et al. Split-spectrum amplitude-decorrelation angiography with optical coherence tomography. Opt Express 2012;20:4710–25.
25. Jia Y, Morrison JC, Tokayer J, et al. Quantitative OCT angiography of optic nerve head blood flow. Biomed Opt Express 2012;3:3127–37.
26. Mansouri K, Medeiros FA, Marchase N, et al. Assessment of choroidal thickness and volume during the water drinking test by swept-source optical coherence tomography. Ophthalmology 2013;120:2508–16.
27. Yasuno Y, Hong Y, Makita S, et al. In vivo high-contrast imaging of deep posterior eye by 1-microm swept source optical coherence tomography and scattering optical coherence angiography. Opt Express 2007;15:6121–39.
28. Zhang C, Tatham AJ, Medeiros FA, et al. Assessment of choroidal thickness in healthy and glaucomatous eyes using swept source optical coherence tomography. PLoS One 2014;9:e109683.
29. Kiumehr S, Park SC, Syril D, et al. In vivo evaluation of focal lamina cribrosa defects in glaucoma. Arch Ophthalmol 2012;130:552–9.
30. Hodapp E, Parrish RK II, Anderson DR. Clinical decisions in glaucoma. St Louis: The CV Mosby Co; 1993:52–61.
31. Cohen J. Weighted kappa: nominal scale agreement with provision for scaled disagreement or partial credit. Psychol Bull 1968;70:213–20.
32. Landis JR, Koch GG. An application of hierarchical kappa-type statistics in the assessment of majority agreement among multiple observers. Biometrics 1977;33:363–74.
33. Burgoyne CF. A biomechanical paradigm for axonal insult within the optic nerve head in aging and glaucoma. Exp Eye Res 2011;93:120–32.
34. Mackenzie PJ, Cioffi GA. Vascular anatomy of the optic nerve head. Can J Ophthalmol 2008;43:308–12.
35. Guidoboni G, Harris A, Carichino L, et al. Effect of intraocular pressure on the hemodynamics of the central retinal artery: a mathematical model. Math Biosci Eng 2014;11:523–46.
36. Guidoboni G, Harris A, Cassani S, et al. Intraocular pressure, blood pressure, and retinal blood flow autoregulation: a mathematical model to clarify their relationship and clinical relevance. Invest Ophthalmol Vis Sci 2014;55:4105–18.
37. Henkind P. Radial peripapillary capillaries of the retina. I. Anatomy: human and comparative. Br J Ophthalmol 1967;51:115–23.
38. Henkind P, Bellhorn RW, Poll D. Radial peripapillary capillaries. 3. Their development in the cat. Br J Ophthalmol 1973;57:595–9.
39. Kornzweig AL, Eliasoph I, Feldstein M. Selective atrophy of the radial peripapillary capillaries in chronic glaucoma. Arch Ophthalmol 1968;80:696–702.
40. Yu PK, Cringle SJ, Yu DY. Correlation between the radial peripapillary capillaries and the retinal nerve fibre layer in the normal human retina. Exp Eye Res 2014;129:83–92.
41. Perneger TV. What's wrong with Bonferroni adjustments. BMJ 1998;316:1236–8.
42. Benjamini Y, Hochberg Y. Controlling the false discovery rate: a practical and powerful approach in multiple testing. J R Stat Soc Series B Stat Methodol 1995;57:289–300.

Footnotes and Financial Disclosures

Originally received: March 15, 2016.
Final revision: July 5, 2016.
Accepted: July 12, 2016.
Available online: ■■■. Manuscript no. 2016-553.

[1] Hamilton Glaucoma Center, Shiley Eye Institute, and the Department of Ophthalmology, University of California San Diego, La Jolla, California.

[2] Department of Ophthalmology, Haeundae Paik Hospital, Inje University College of Medicine, Busan, South Korea.

Financial Disclosure(s):
The author(s) have made the following disclosure(s): L.M.Z.: Research support − Carl Zeiss Meditec, Heidelberg Engineering, National Eye Institute, and Topcon.

F.A.M.: Financial support − Alcon, Allergan, Bausch & Lomb, Carl Zeiss Meditec, Heidelberg Engineering, Merck, Reichert, Sensimed, and Topcon; Research support − Alcon, Allergan, Carl Zeiss Meditec, National Eye Institute, and Reichert; Consultant − Allergan, Carl Zeiss Meditec, and Novartis.

R.N.W.: Research support − Carl Zeiss Meditec, Genentech, Heidelberg Engineering, National Eye Institute, Optovue, and Topcon; Consultant − Alcon, Allergan, Bausch & Lomb, Carl Zeiss Meditec, Sensimed, and Topcon.

Supported in part by National Institutes of Health/Nation Eye Institute grants P30EY022589, EY11008, EY019869, and EY021818; a grant from research year of Inje University in 2015; and an unrestricted grant from Research to Prevent Blindness (New York, NY). The funding organizations had no role in the design or conduct of this research.

Author Contributions:

Conception and design: Suh, Zangwill, Weinreb

Data collection: Suh, Zangwill, Manalastas, Belghith, Yarmohammadi, Medeiros, Diniz-Filho, Saunders, Yousefi, Weinreb

Analysis and interpretation: Suh, Zangwill, Manalastas, Belghith, Yarmohammadi, Medeiros, Diniz-Filho, Saunders, Yousefi, Weinreb

Obtained funding: Not applicable

Overall responsibility: Suh, Zangwill, Manalastas, Belghith, Yarmohammadi, Medeiros, Diniz-Filho, Saunders, Yousefi, Weinreb

Abbreviations and Acronyms:
cpRNFL = circumpapillary retinal nerve fiber layer; **cpVD** = circumpapillary vessel density; **dB** = decibels; **DIGS** = Diagnostic Innovations in Glaucoma Study; **IN** = inferonasal; **IOP** = intraocular pressure; **IT** = inferotemporal; **LC** = lamina cribrosa; **MD** = mean deviation; **OCT-A** = optical coherence tomography angiography; **ONH** = optic nerve head; **POAG** = primary open-angle glaucoma; **RNFL** = retinal nerve fiber layer; **SD OCT** = spectral-domain optical coherence tomography; **SSADA** = split-spectrum amplitude-decorrelation angiography; **SS-OCT** = swept-source optical coherence tomography; **ST** = superotemporal; **VF** = visual field.

Correspondence:
Robert N. Weinreb, MD, University of California San Diego, 9500 Gilman Drive, MC 0946, La Jolla, CA 92093. E-mail: rweinreb@ucsd.edu.